Available online at www.sciencedirect.com

ScienceDirect

Procedia Manufacturing 26 (2018) 1034–1040

Procedia MANUFACTURING

www.elsevier.com/locate/procedia

46th SME North American Manufacturing Research Conference, NAMRC 46, Texas, USA

Nano-wear-induced behavior of selective laser melting commercial pure titanium

Nan KANG [a,b] *, Mohamed EL MANSORI [a], Nicolas CONIGLIO [a], Christian CODDET[b]

[a] *MSMP Laboratory, EA-7350Arts et Metiers ParisTechAix en Provence, France*
[b] *ICB UMR 6303, CNRS, Univ. Bourgogne Franche-Comté, UTBM, F-90010 Belfort, France*

* Corresponding author. Tel.: +33 0442938181; fax:+33 0442938115.
E-mail address: nan.kang@ensam.eu

Abstract

In this work, the nano-wear-induced behavior of selective laser melting (SLM) processed commercial pure titanium was investigated under several applied loads from 1 mN to 100 mN. The dense (over 99%) commercial pure titanium sample was manufactured using SLM process with optimized process parameters (900 J m^{-1}). Nano-wear testing was performed on the polished surface of SLM processed commercial pure titanium. The friction coefficient increased from 0.04 to 0.9 as the load increased from 1 mN to 100 mN. Additionally, the sliding behavior changed along with the applied loads, from elastic to plastic and unstable friction behaviors. The elastic-plastic transition appeared at applied load of 50 mN, which was also confirmed by the calculation results. While the applied load ranged between 50 mN and 80 mN (plastic friction), the average friction coefficient was light smaller than that of the macroscopic ball-on-disc test. During the sliding, a friction vibration appeared and its mechanism was also investigated and discussed combine the wear surface morphologies.

Peer-review under responsibility of the scientific committee of the 46th SME North American Manufacturing Research Conference.

Keywords: Selective Laser Melting; pure titanium; Microstructure; nano wear; friction coefficient.

1. Introduction

Additive manufacturing (AM), contrast to conventional subtractive manufacturing process, is one kind of layer by layer joint manufacturing, which presents immanent advantages, such as unrivalled design freedom and short lead time. Selective laser melting (SLM), powder-bed laser additive manufacturing, is one of the important net-shaped manufacturing technologies [1]. In this process, the component is firstly design in 3D model using a computer-aided design (CAD) software, after that, this model is divided into 2D layer with very low thickness (from 20 μm to 100 μm). And then a

2351-9789
Peer-review under responsibility of the scientific committee of the 46th SME North American Manufacturing Research Conference.
10.1016/j.promfg.2018.07.136

computer controlled high power focused laser selectively scan the powder bed, the laser scanned powder is fully melted and rapid solidified. As it finished, the build platform descends by one layer thickness and then a new layer of powder is deposited on top. In recent year, SLM has become an attractive additive manufacturing process with distinct advantages in manufacturing accuracy and complex geometry shape [2], because the laser energy source could be easily focused on several micrometers with economical optical system for obtaining the high energy density [3]. Moreover, as one of the powder-bed manufacturing, the untreated powder acts as support part during the construction, which significantly enhances the fabricating flexibility. Until now, wide ranges of materials have been successfully prepared by SLM, such as metals, ceramics and polymers [4-7]. As one result of low interaction volume, high energy density and free surface, the cooling rate of melting pool in SLM process is superior to 10^5 K/s, which leads to the ultra-fine or metastable microstructure. For instance, in the work of K. D. Ralston and N. Birbilis [8], the SLM processed alloys exhibit higher strength, wear/corrosion resistance than that of conventional casted sample.

Consideration of high machining costs and long lead times in conventional process, Ti and Ti alloys are widely considered to be manufactured by SLM. The commercial pure titanium (CP-Ti) is used for a great variety of applications, such as bio-technology, given to its low density, high strength, corrosion resistance and biocompatibility [9]. Therefore, SLM process presents irreplaceable advantage in manufacturing of metallic implantation. SLM processed CP-Ti, thus, was extensive studies [10-14] with focus on the microstructure and mechanical properties. However, for the normal implantation materials, the functional properties are determined mainly by surficial characterizations, such as, biocompatibility, roughness, hardness, and wear/corrosion resistance. Until now, few works direct at the surface properties, especially nano-scale, of SLM processed CP-Ti. Gu et al. [10] analysis the nano-hardness of SLM processed CP-Ti and reported the appearance of martensitic α' reinforcement. Attar et al. [14] compared the wear behavior of SLM processed and conventional casted CP-Ti. They reported that the wear resistance of SLM processed sample is high than that of casted sample. From the view of applications, the implants made of pure titanium are expected to operate suitably in the nano-wear regime (low wear rates), where a negligible amount of material is removed per movement. Furthermore, the wear behavior changes in the various wear regimes, on account of nonlinear nature of wear processes. Therefore, the knowledge of macro-wear behavior is not helpful to understand the wear mechanisms that operate in the nano regime [15].

The objective of this study is to investigate nano-wear induced behavior of SLM processed CP-Ti sample under several applied loads. The possible wear mechanism in function of applied load was proposed and discussed, which can be employed to understand the surface wear behavior of SLM processed sample under several loads.

2. Methods and experimental details

A home-made CP-Ti powder (gas-atomization) was used in this study, which presents a particular irregular morphology (see in Fig. 1 (a)). As shown in Fig. 1 (b), the laser diffraction result shows a mean particle size of 41.7 μm with a normal distribution. The as fabricated samples, which was contracted on the TC4 (Ti6Al4V) substrate, is shown in Fig. 1 (c).

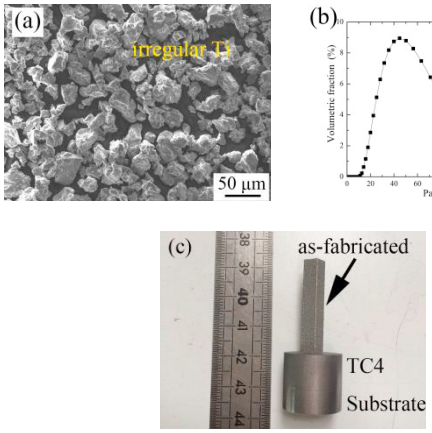

Fig. 1. (a) Morphology and (b) particle size distribution of CP-Ti powder (c) as-fabricated cubic samples.

Commercial SLM 250 apparatus (MCPHEK Tooling GmbH, Germany) equipped with an Nd-YAG fiber laser (spot size, 40 μm and maximum power, 400W) was employed to prepare the sample. In this work, in order to obtain high density parts. Laser power, laser scanning speed, layer thickness and hatch distance, were respectively set at 175 W, 1.25 m/s, 110 μm and 50 μm. In general, the high

layer thickness improves the manufacturing efficiency. However, as the layer thickness increases, the required melting volume increases rapidly. Due to the limitation of input energy density, the optimized layer thickness in work is about 50 µm for CP-Ti. Indeed, the SLM processed Ti part is processed under the optimized parameters [16, 17] with energy density (900 J m^{-1}), which is defined as follow:

$$E_\rho = \frac{P_{(power)}}{V_{(scanning)}} \quad (1)$$

Where E_ρ is energy density (J m^{-1}),
P is laser power (W)
v is laser scanning speed (m s^{-1}).

The laser scanning mode is a single melt scanning strategy with a scanning rotation of 90° between successive layers, which is schematically illustrated in Fig. 2.

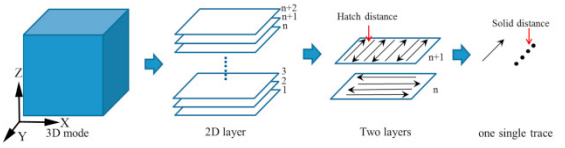

Fig. 2 Schematic illustration of SLM process (BD, building direction Z, SD_x scanning direction X, SD_y scanning direction Y).

The microstructure was characterized by X-ray diffraction (XRD), optical microscopy (OM) and Scanning Electron Microscopy (SEM). A nano-wear system (Morphoscan machine of Michalex, see in Fig. 3 (a)) with a spherical diamond indenter (10-µm diameter) was used to measure the surface mechanical properties. The SLM processed sample slide under a still indenter. The sliding distance and speed were set at 500 µm and 2 µm s^{-1}. As shown in Fig. 3 (b), the test sequence is preprogramed with multiple-pass test process [18]:

(1) Wear length definition in Y+ direction:
Indenter moved with the sliding distance of 600 µm at 0.2 mN.
(2) Initial topography scan (in Y- direction):
Indenter moved back to initial position under very-low force of 0.2 mN.
(3) Upload-wear-unload cycle (in Y+ direction):
(3.1) indenter moved 50 µm under very low load of 0.2 mN and then charged to a high load (between 1 and 100 mN).
(3.2) indenter moved 500 µm at 2µm/s and then discharged.
(3.3) indenter moved 50 µm under very low load of 0.2mN.
(4) Final topography scan (in Y- direction):
Indenter moved back to initial position under very-low load of 0.2 mN.
(5) Data analysis;

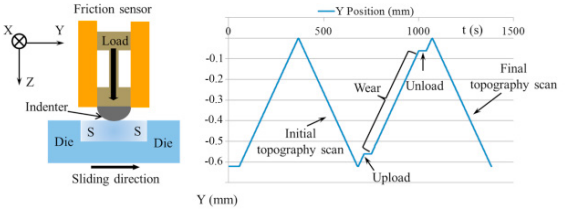

Fig. 3. Schematic illustration of nano-wear test (S: substrate).

3. Results and discussions

The XRD patterns of raw powder and SLM processed CP-Ti is shown in Fig. 4. Firstly, only the titanium phase is observed with main phase of (1 0 1) plane for both powder and SLM processed sample. Moreover, compared with the standard peak position of CP-Ti phase, the SLM processed sample presents a small movement to right direction. It indicates that a phase transition from α-Ti to martensitic α' Ti appears in the SLM processed CP-Ti, due to high cooling rate [10].

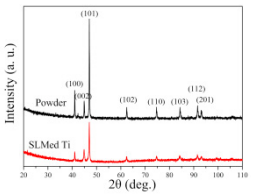

Fig.4. XRD patterns of powder and SLM processed commercial pure titanium

The microstructures after chemical attaching from top and side views of SLM processed CP-Ti are shown in Fig. 5. From the figures, some porosity smaller than 5 µm in diameter could be observed with spherical morphology at both top and side views (see in Fig. 5 (a and b)). According to the report of Kasperovich et al. [16, 17], the spherical small pores are formed during the melting process with inert gas cladding. Moreover, the image analysis indicates that the porosity of SLM processed CP-Ti sample is inferior to 0.5%. Additionally, it can be seen that

some grey needle-liked grains appear on the top and side views, which is supposed to be martensitic α'-Ti [10]. In general, the transition from β to α phase happens at temperature around 882 °C in the case of low cooling rates, where the α phase illustrates the regular lath-shaped grains. But, as the cooling rate increase, the β phase tend to transfer as martensitic α' phase, which present a refined acicular shape. Moreover, attributed to layer by layer manufacturing process, the SLM processed alloys present anisotropic thermal gradient, microstructure and mechanical properties [18, 19]. During the SLM process, the surrounding material, for example thermal conductivity of powder and solidified material near molten pool affects significantly the temperature gradient. So, the heat conduction in building direction is higher than that of spatial directions. As the results of cooling rate controlled martensitic transition, the acicular α' phase grow along the high temperature gradient building direction (see in Fig. 5 (c and d)).

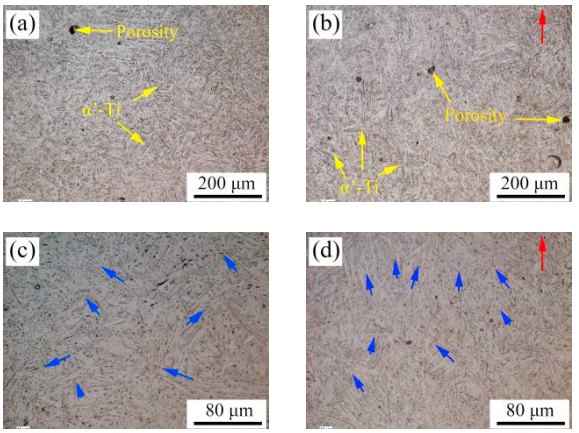

Fig. 5. OM images of SLM processed CP-Ti (a, c) top view and (b, d) side view (build direction indicated by red arrow).

The nano-wear test was performed and the friction coefficients (CoF) and penetration depth in function of applied loads are shown in Fig. 6. As seen in Fig. 6 (a), the CoF can be divided into 4 stages: (I) variant low CoF (morphological friction); (II) low CoF (elastic friction); (III) high CoF (plastic friction) and (IV) unstable high CoF (unstable friction). When the applied load is inferior to 10 mN, the CoF ranged between 0.02 and 0.1 with a light fluctuation. Due to small penetration depths (<50 nm, in Fig. 6 (b)), which is smaller than polishing roughness, the surface morphology leads to the CoF fluctuation. Moreover, the constraint applied on the surface on polished surface could be calculated by the equation:

$$\sigma = 0.102 \times \frac{2F}{\pi D(D - \sqrt{D^2 - d^2})} \quad (2)$$

Where, F is applied load; D is indenter diameter; d is diameter of indentation, which is associated to penetration p (in case of $2p<D$):

$$d^2 = D^2 - (D - p)^2 \quad (3)$$

According to the equations (2) and (3),

$$\sigma = 0.102 \times \frac{2F}{\pi D p} \quad (4)$$

As reported by Attar et. al. [20], the elastic resistance of SLM processed CP-Ti is about of 560 MPa. Thus, from the equation (4), it can be calculated the elastic-plastic transition (EPT) appears at applied load of 50 mN, which can also be observed in Fig. 6 (a) between stage II and III. Moreover, the stage III shows larger fluctuation than that of stage II. As the applied load increases to 80 mN, the CoF raises from 0.3 to 0.9. Additionally, the fluctuation of CoF increases significantly from 0.2 to 2 (stage IV in Fig 6 (a)). On the other hand, the penetration depth increases linearly with the increment of applied loads (see in Fig. 6 (b)).

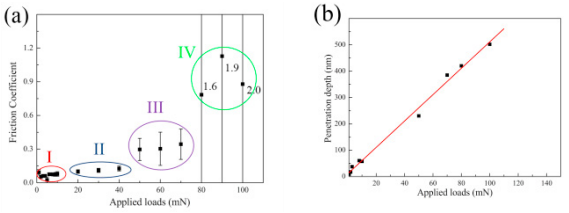

Fig. 6. (a) Average friction coefficient (number in Figure indicates the variance) (b) penetration depth of SLM processed CP-Ti under several applied loads (penetration depth is measured under maximum load force).

Fig. 7 presents the detailed analysis of the CoF under loads from 1 mN to 100 mN. It can be seen from Fig. 7 (a and b) that the CoF is stable with a standard deviation below 0.1 for applied load smaller than 50 mN (morphological and elatic friction). As the applied load increased to 50 mN (plastic friction), fluctuations appeared all along the sliding trace (see Fig. 7 (c)). The similar phenomena was also present in the case of macro-wear behavior for SLM processed Ti [21]. In macro-scale, it could be

attributed to two factors: (1) the roughness and (2) cold welding effect. However, in this work, the one pass sliding on the polished (Ra<0.1 μm) surface and low sliding speed could significantly reduce the effects of those two factors. A possible wear mechanism is illustrated in Fig. 9. In this mode, the materials stripped step by step during the sliding process at the plastic and unstable friction stages. Thus, the lateral load (friction coefficient) also presented some fluctuations. As shown in Fig. 7 (d), when the applied load was about 100 mN, a large friction coefficient value (about of 9) appears at the beginning of sliding. As the material is stripped, the friction coefficient decreases rapidly to about 0.3.

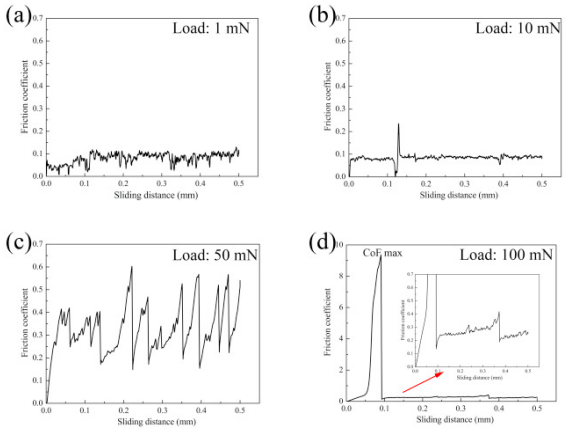

Fig. 7. Friction coefficient of SLM processed CP-Ti under different loads (a) 1 mN, (b) 10 mN, (c) 50 mN and (d) 100mN.

The worn surfaces under several loads ranged from 1 mN to 100 mN of SLM processed Ti are shown in Fig. 8. The overview image (Fig. 8 (a)) shows that the wear traces can be observed by SEM at the condition of applied load superior 50 mN. This phenomenon is well confirmed by calculated results as mentioned above. The local view of wear traces are shown in Fig. 8 (b and c) in cases of applied load of 90 mN and 100 mN, which are located in Fig. 8 (a) by red arrows. Under an applied load of 100 mN, the fracture surface can be seen at the beginning of wear trace and then following a shallow wear trace (see in Fig. 8 (b)). As shown in Fig. 8 (c), when the applied load drops to 90 mN, the wear trace is continuous with discontinuous extrusion. The 3-D image and cross sectional profiles of wear trace are shown in Fig. 8 (d and e). The cross sectional profile positions are indicated in Fig. 8 (d) with A-A and B-B. It can be concluded that the depth of wear trace is not uniform and ranged from 200 nm to 400 nm. Additionally, the cross-sectional circular profile B-B indicates the ratio of wear trace is about of 10 μm, which is in agreement with the spherical indenter.

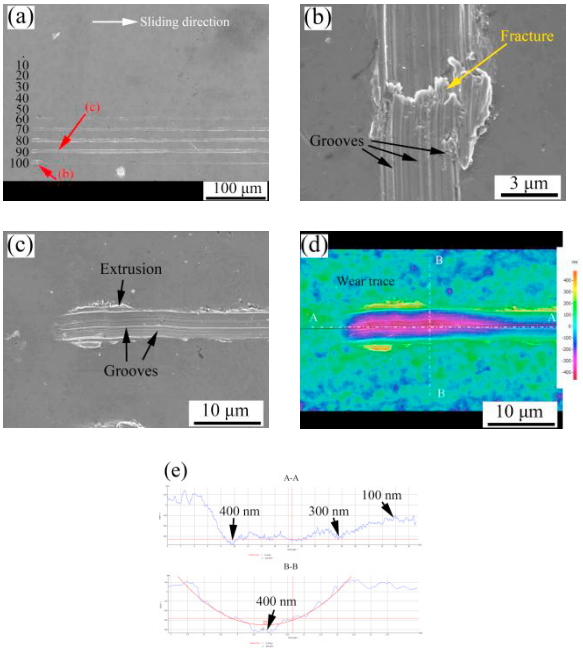

Fig. 8 (a) The worn surface under several applied loads ranged from 1 mN to 100 mN, local view of worn surface under applied loads of (b) 100 mN and (c) 90 mN and the corresponding (d) 3D image and (e) section profile.

The wear mechanism of SLM processed CP-Ti under several loads are shown in Fig. 8. In the case of mild load (Fig. 9 (a)), no elastic/plastic deformation of substrate was obviously realized. The penetration depth of the indenter was inferior to 10 nm from Fig. 5 (b). The indenter, thus, acted as a probe to determine the surface morphology. As the applied load increased to normal situation (Fig. 9 (b)), a penetration of hundreds nanometers appeared on substrate surface. During the sliding process, the lateral material was deformed and accumulated. So, the lateral load increased simultaneously. On account of the positive correlation between lateral load and friction coefficient, the friction coefficient increases too. With this trend, a stress concentration is formed near the indenter, which leads to cracks and fracture. As one of the results of local fracture, the friction coefficient decreased rapidly. Therefore, a fluctuation of friction could be observed in sample with normal load (Fig. 7 (c)). However, if the substrate is overloaded (severe load > 80 mN, Fig. 9 (c)), larger lateral force is required to realize the fracture of the

material, because of the large penetration depths associated. Therefore, the maximum friction coefficient increased to about 10 with one peak (Fig. 9 (d)) at the beginning of trace, which indicated that the damage mechanism changes from wear to scratch. Meanwhile, the indenter is also bended during the sliding process. When the cracks and fracture appear, the indenter goes immediately back to no-loaded position due to low lateral load. So, the Cof decreases very rapidly. Therefore, the wear mechanism changes from elastic, plastic to unstable (scratch), as the applied loads increases.

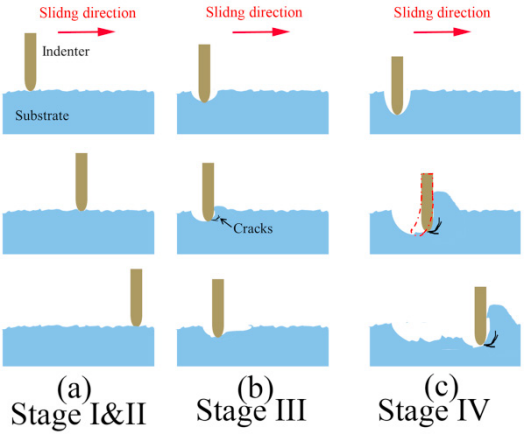

Fig. 9 Illustration of nano wear of SLM processed CP-Ti under several loads (a) mild, (b) normal and (c) severe.

4. Conclusion

In summary, dense commercial pure titanium (CP-Ti) components were manufactured by selective laser melting (SLM) process. The nano-wear induced behavior of SLM processed CP-Ti was investigated. Based on microstructural characterizations and nano-wear behaviors, some conclusions were reached:

(1) The SLM processed CP-Ti showed a mixed microstructure of lath α *hcp* Ti and acicular α' hcp Ti.

(2) As the applied load increases from 1 to 100 mN, the friction coefficient increased from 0.05 to 0.9. Meanwhile, the sliding behavior changed from elastic, plastic to unstable friction. Their potential application changed also from topography detector to wear and scratch damages.

(3) The elastic-plastic transition of friction behavior appeared at applied load of 50 mN.

(4) In the case of plastic friction, the friction coefficient nano-wear was smaller than that of micro-wear test [21].

(5) Moreover, the fluctuation of CoF was also observed during nano-wear process. A possible damaging mechanism was proposed based on material stripping behavior. This mechanism could be used during the micro and macro sliding test to understand the incipient stage of damages.

References

[1] C.Y. Yap, C.K. Chua, Z.L. Dong, Z.H. Liu, D.Q. Zhang, L.E. Loh, S.L. Sing, Review of selective laser melting: Materials and applications, Appl. Phys. Rev. 2 (2015) 041101.

[2] N. Kang, P. Coddet, J. Wang, H. Yuan, Z. Ren, H. Liao, C. Coddet, A novel approach to in-situ produce functionally graded silicon matrix composite materials by selective laser melting, Compos. Struct. 172 (2017) 251–258..

[3] E.O. Olakanmi, R.F. Cochrane, K.W. Dalgarno, A review on selective laser sintering/melting (SLS/SLM) of aluminium alloy powders: Processing, microstructure, and properties, Prog. Mater. Sci. 74 (2015) 401–477.

[4] B. Song, Z. Wang, Q. Yan, Y. Zhang, J. Zhang, C. Cai, Q. Wei, Y. Shi, Integral method of preparation and fabrication of metal matrix composite: selective laser melting of in-situ nano/submicro-sized carbides reinforced iron matrix composites, Mater. Sci. Eng. A. 707 (2017) 478–487.

[5] N. Kang, P. Coddet, C. Chen, Y. Wang, H. Liao, C. Coddet, Microstructure and wear behavior of in-situ hypereutectic Al-high Si alloys produced by selective laser melting, Mater. Des. 99 (2016) 120–126.

[6] N. Shen, A. Samanta, Q. Wang, H. Ding, Selective Laser Melting of Fiber-Reinforced Glass Composites, Manuf. Lett. 14 (2017) 6–9.

[7] M. Schmidt1, D. Pohle, T. Rechtenwald, Selective Laser Sintering of PEEK, Annals of the CIRP, 56 (2007) 205-208.

[8] K. D. Ralston, N. Birbilis, Effect of Grain Size on Corrosion: A Review, Corrosion. 2010, 66(7):075005-075005-13.

[9] E.O. Ezugwu, Z.M. Wang, Titanium alloys and their machinability, J. Mater. Process. Technol. 68 (1997) 262–274.

[10] D. Gu, Y.C. Hagedorn, W. Meiners, G. Meng, R.J.S. Batista, K. Wissenbach, R. Poprawe, Densification behavior, microstructure evolution, and wear performance of selective laser melting processed commercially pure titanium, Acta Mater. 60 (2012) 3849–3860.

[11] B. Zhang, H. Liao, C. Coddet, Microstructure evolution and density behavior of CP Ti parts elaborated by Self-developed vacuum selective laser melting system, Appl. Surf. Sci. 279 (2013) 310–316.

[12] Y. Li, D. Gu, Thermal behavior during selective laser melting of commercially pure titanium powder: Numerical simulation and experimental study, Addit. Manuf. 1 (2014) 99–109.

[13] Fischer, V. Romano, H.P. Weber, N.P. Karapatis, E. Boillat, R. Glardon, Sintering of commercially pure titanium powder

with a Nd:YAG laser source, Acta Mater. 51 (2003) 1651–1662.
[14] H. Attar, K.G. Prashanth, A.K. Chaubey, M. Calin, L.C. Zhang, S. Scudino, J. Eckert, Comparison of wear properties of commercially pure titanium prepared by selective laser melting and casting processes, Mater. Lett. 142 (2015) 38–41.
[15] R.L. Deuis, C. Subramanian, J.M. Yellupb, Dry Sliding Wear of Aluminium Composites-a Review, Compos. Sci. Technol. 57 (1997) 415–435.
[16] G. Kasperovich, J. Haubrich, J. Gussone, G. Requena, Correlation between porosity and processing parameters in TiAl6V4 produced by selective laser melting, Mater. Des. 105 (2016) 160–170.
[17] K.V. Yang, P. Rometsch, T. Jarvis, J. Rao, S. Cao, C. Davies X.H. Wu, Porosity formation mechanisms and fatigue response in Al-Si-Mg alloys made by selective laser melting, Mat Sci Eng A-Struct, 712 (2018) 166–174.
[18] N. Kang, H. Yuan, P. Coddet, Z. Ren, C. Bernage, H. Liao, C. Coddet, On the texture, phase and tensile properties of commercially pure Ti produced via selective laser melting assisted by static magnetic field, Mater. Sci. Eng. C. 70 (2017) 405–407
[19] T. Vilaro, C. Colin, J.D. Bartout, As-fabricated and heat-treated microstructures of the Ti-6Al-4V alloy processed by selective laser melting, Metall. Mater. Trans., A 42 (2011) 3190-3199.
[20] H. Attar, M. Bönisch, M. Calin, L.C. Zhang, S. Scudino, J. Eckert, Selective laser melting of in situ titanium-titanium boride composites: Processing, microstructure and mechanical properties, Acta Mater. 76 (2014) 13–22.
[21] N. Kang, P. Coddet, Q. Liu, H.L. Liao, C. Coddet, In-situ TiB/near α-Ti matrix composites manufactured by selective laser melting, Addit. Manuf. 11 (2016) 1–6.